

# The roles of autophagy and hypoxia in human inflammatory periapical lesions

H. Y. Huang<sup>1,2,†</sup>, W. C. Wang<sup>2,3,4,†</sup>, P. Y. Lin<sup>1</sup>, C. P. Huang<sup>1</sup>, C. Y. Chen<sup>2,3,4</sup>  
& Y. K. Chen<sup>2,3,4</sup> 

<sup>1</sup>Department of Dentistry, Ditmanson Medical Foundation Chia-Yi Christian Hospital, Chia-Yi; <sup>2</sup>School of Dentistry, College of Dental Medicine, Kaohsiung Medical University, Kaohsiung; <sup>3</sup>Oral & Maxillofacial Imaging Center, College of Dental Medicine, Kaohsiung Medical University, Kaohsiung; and <sup>4</sup>Division of Oral Pathology & Maxillofacial Radiology, Department of Dentistry, Kaohsiung Medical University Hospital, Kaohsiung, Taiwan

## Abstract

**Huang HY, Wang WC, Lin PY, Huang CP, Chen CY, Chen YK.** The roles of autophagy and hypoxia in human inflammatory periapical lesions. *International Endodontic Journal*, 51, e125–e145, 2018.

**Aim** To determine the expressions of hypoxia-related [hypoxia-inducible transcription factors (HIF)-1 $\alpha$ , BCL2/adenovirus E1B 19 kDa protein-interacting protein 3 (BNIP3) and phospho-adenosine monophosphate activated protein kinase (pAMPK)] and autophagy-related [microtubule-associated protein 1 light chain 3 (LC3), beclin-1 (BECN-1), autophagy-related gene (Atg)5–12, and p62] proteins in human inflammatory periapical lesions.

**Methodology** Fifteen samples of radicular cysts (RCs) and 21 periapical granulomas (PGs), combined with 17 healthy dental pulp tissues, were examined. Enzyme-linked immunosorbent assay (ELISA) was used to detect interleukin (IL)-1 $\beta$  cytokine; immunohistochemical (IHC) and Western blot (WB) analyses were employed to examine autophagy-related and hypoxia-related proteins. Transmission electron microscopy (TEM) was used to explore the ultrastructural

morphology of autophagy in periapical lesions. Non-parametric Kruskal–Wallis tests and Mann–Whitney *U*-tests were used for statistical analyses.

**Results** ELISA revealed a significantly higher ( $P < 0.001$ ) IL-1 $\beta$  expression in periapical lesions than in normal pulp tissue. Immunoscopes of IHC expressions of pAMPK, HIF-1 $\alpha$ , BNIP3, BECN-1 and Atg5–12 proteins in periapical lesions were significantly higher ( $P < 0.001$ ) (except BECN-1) than those in normal pulp tissue. The results of IHC studies were largely compatible with those of WB analyses, where significantly higher ( $P < 0.05$ ) expressions of hypoxia-related and autophagy-related proteins (except BECN-1, p62 and LC3II in WB analyses) in periapical lesions were noted as compared to normal pulp tissue. Upon TEM, ultrastructural double-membrane autophagosomes and autolysosomes were observed in PGs and RCs.

**Conclusions** Autophagy associated with hypoxia may play a potential causative role in the development and maintenance of inflamed periapical lesions.

**Keywords:** autophagy, hypoxia, inflammation, periapical granuloma, radicular cyst.

Received 6 September 2016; accepted 20 April 2017

Correspondence: Yuk-Kwan Chen, School of Dentistry, College of Dental Medicine, Kaohsiung Medical University, Kaohsiung, Taiwan (e-mail: yukkwa@kmu.edu.tw).

<sup>†</sup>The first two authors contributed equally to this study.

## Introduction

Inflammatory periapical lesions, including radicular cysts (RCs) and periapical granulomas (PGs), are part of the body's defence response to the threat of microbial invasion in root canals. With persistent infection sources via root canals, inflammatory periapical

lesions cannot heal and therefore persist (Lin *et al.* 2009). According to the various theories of cystic formation, ischaemia hypoxia and nutrient depletion are considered to exist in the central areas of the inflamed periapical lesions (Nair *et al.* 2008). The hypoxia and inflammatory environments may induce angiogenic processes (Konisti *et al.* 2012), cell proliferation or cell protection through several mechanisms such as autophagy to help cells overcome this challenging situation (Mazure & Pouyssegur 2010).

Autophagy is an evolutionally conserved self-degradation pathway occurring in the cytoplasm of eukaryotic cells. By generating an unique double-membrane vacuoles, damaged DNAs, dysfunctional proteins or injured organelles could be dissociated into nucleotides, amino acids or fatty acids, which are then recycled to produce macromolecules and adenosine triphosphates (ATPs) required to support the fundamental life of cells (Ravikumar *et al.* 2009). Therefore, autophagy plays a critical role in energy supply under stressful, starved or hypoxic conditions, and also in physiological cellular homeostasis. Worthy of note, autophagy interacts with inflammation and immune responses and upregulation or downregulation of autophagy is potentially related to the development of several pathogenic diseases such as tumorigenesis and neurodegeneration (Kamada *et al.* 2004, Eskelinen 2005, Rubinsztein *et al.* 2011).

During autophagy, several genes and proteins participate in forming four major stages: nucleus complex formation, elongation of double membrane, formation of autophagosomes and finally fused with lysosome to become autolysosomes. At first, beclin-1 (BECN-1) is a key protein involved in nucleus complex formation and creates a section of double membrane; then, autophagy-related gene (Atg)5–12 complex, microtubule-associated protein 1 light chain 3 (LC3) and p62 are related to the elongation of the membrane, forming autophagosomes and wrapping up the targeted proteins or organelles to lysosomes (Rabinowitz & White 2010).

Additionally, hypoxia-induced autophagy can be initiated by two separate pathways. The main process is through a hypoxia-inducible transcription factor (HIF)-1 $\alpha$ -dependent adaptive pathway with induction of BCL2/adenovirus E1B 19 kDa protein-interacting protein 3 (BNIP3), a BH3-only protein, which could release free BECN-1 by competing the binding of Bcl-2/BECN-1 complex, and then inducing the following autophagic processes. It has been demonstrated that hypoxic stimuli can enhance HIF-1 $\alpha$  protein

production, which is known to increase cell proliferation and a predominant mediator of cellular adaptation to hypoxia (Dery *et al.* 2005). Furthermore, inflammation (e.g. LPS-mediated inflammation, interleukin (IL)-1 $\beta$ ) is another microenvironmental factor that can stimulate HIF-1 signalling (Hellwig-Burgel *et al.* 1999, Blouin *et al.* 2004). Another is a HIF-1 $\alpha$ -independent pathway, namely the adenosine monophosphate-activated protein kinase (AMPK)/mammalian target of rapamycin (mTOR) pathway (Mazure & Pouyssegur 2010). AMPK is also an important cellular response to maintain energy homeostasis under low oxygen. Through suppressing the mTOR kinase, activated AMPK phosphate could also induce autophagy (Zhou *et al.* 2012).

Recent studies revealed that autophagy of human dental pulp cells has a cytoprotective role against hypoxic stress through the AMPK/mTOR pathway (Zhou *et al.* 2013), and autophagy has also demonstrated in human inflamed periapical lesions (Zhu *et al.* 2013). The potential role of autophagy and hypoxia environments related to the development of human inflammatory periapical lesions has not yet been elucidated. Based on the above description, it can be hypothesized that autophagy could participate in the development of human inflammatory periapical lesions associated with expression of HIF-1 $\alpha$ /BNIP3 or AMPK/mTOR. Hence, this study aimed to investigate the expressions of hypoxia-related proteins (HIF-1 $\alpha$ , BNIP3 and pAMPK) and autophagy-related proteins (BECN1, Atg5–12, LC3, and p62) in inflamed periapical lesions in order to explore the potential contribution of autophagy and hypoxia environments related to the pathogenesis of inflamed periapical lesions. The null hypothesis is autophagy, and hypoxia-related proteins are not present in human inflammatory periapical lesions.

## Materials and methods

### Tissue samples collection

All tissue samples in the study were obtained from patients who visited the Dental Department of Ditmanson Medical Foundation Chia-Yi Christian Hospital, Taiwan, following informed consent in line with the rules of the Institutional Review Board (IRB: CYCH-103008).

A total of 53 patients (26 males and 27 females; mean age: 40.6 years, ranging from 20 to 74 years) were collected (Table 1). Specimens were obtained

from inflamed periapical lesions or healthy/normal dental pulp undergoing periapical surgery or tooth extraction. The samples contained 15 radicular cyst (RC) patients (eight males and seven females; mean age: 48.5 years, ranging from 21 to 66 years), 21 periapical granuloma (PG) patients (nine males and 12 females; mean age: 45 years, ranging from 20 to 74 years), and 17 adult patients (nine males and eight females; mean age: 28.2 years, ranging from 20 to 61 years) with normal dental pulp tissues who underwent third-molar extraction due to surgical indications. Diagnoses of inflamed periapical lesions were based on the criteria of the World Health Organization with respect to histopathology, clinical history and radiographic appearance. Hence, the criteria for RCs were defined as: (i) a lesion located in the periapical region of a tooth with a necrotic pulp without periodontal communication, and (ii) RC demonstrated a cystic cavity surrounded by a nonkeratinizing epithelial lining, with inflammatory cells in the connective tissue. The criteria for PGs were defined as follows: (i) a lesion located in the periapical region of a tooth with a necrotic pulp without periodontal communication; and (ii) histologic examination showed no epithelial cells, but filling with infiltrating inflammatory cells was noted (macrophages, lymphocytes, PMNs and plasma cells). Patients with teeth with sinus tracts, severe periodontitis and those who had received previous apical surgery were excluded. On the other hand, all normal pulp tissues were obtained from extracted teeth without caries and signs of periapical periodontitis. The pulpal tissues were retrieved immediately by resecting the extracted tooth using a sterile high-speed fissure bur.

Additionally, the inflamed periapical lesions were subdivided into those measuring fewer than and those of more than  $10^2 \text{ mm}^2$  in size, as detected by periapical radiographic examination (Table 2).

**Table 1** Demographic data of the patients in the current study

Types of samples	Male	Female	Mean age $\pm$ standard deviation (years)	Total cases
Periapical granuloma	9	12	45 $\pm$ 14.6	21
Radicular cyst	8	7	48.5 $\pm$ 14.0	15
Normal pulp tissue	9	8	28.2 $\pm$ 12.1	17
Total cases	26	27	40.6 $\pm$ 16.0	53

**Table 2** Classification of lesion size on periapical radiographic examination

Groups	$\leq 10^2 \text{ mm}^2$	$> 10^2 \text{ mm}^2$	Total cases
Periapical granuloma	16 (76.2%)	5 (23.8%)	21
Radicular cyst	9 (60.0%)	6 (40.0%)	15
Total cases	25	11	36

A portion of each sample of the periapical lesions (PGs and RCs) and normal pulp tissues was fixed in 10% neutral-buffered formalin for immunohistochemical (IHC) staining, and the remaining portions were stored immediately in liquid nitrogen for subsequent enzyme-linked immunosorbent assay (ELISA) and Western blot (WB) analyses.

### Extraction of proteins from tissues

Tissue samples (25–40 mg) from each of PGs, RCs and normal pulp were, respectively, inserted into a 2-mL sterile tube containing six to seven pieces of ceramic beads. Then, 400  $\mu\text{L}$  of protein extraction reagent [T-PER<sup>®</sup> Tissue Protein Extraction Reagent (Thermo, Glen Burnie, MD, USA) mixed with Halt<sup>™</sup> Protease Inhibitor Cocktail (Thermo), 10 : 1] was added into the tube, and the contents were briefly vortexed, followed by processing with a robust and high-throughput homogenizer (Precellys 24, bertin, Montigny-le-Bretonneux, France) under the following conditions: (i) speed: 6000 rpm; (ii) homogenization duration: 30 s; (iii) number of cycles: at least five cycles until most tissues were disrupted.

After each cycle, the tube was removed from the homogenizer and placed on ice for 1 min in order to cool the dissected tissues. The samples then underwent another cycle until homogenization was achieved, as confirmed by a visual check.

The supernatant was then transferred to a new tube and centrifuged at 17 970  $g$  for 30 min at 4 °C to settle the remaining insoluble material. The supernatant containing lysis proteins was subsequently aspirated into a fresh Eppendorf tube, which was immediately stored at  $-80 \text{ }^\circ\text{C}$  for subsequent ELISA and WB analyses.

### Enzyme-linked immunosorbent assay

An ELISA kit (human IL-1 $\beta$  ELISA MAX<sup>™</sup> Deluxe) was purchased from BioLegend (San Diego, CA, USA; Cat. No. 437004). A primary antibody was first coated on a 96-well plate by adding 100  $\mu\text{L}$  diluted

human IL-1 $\beta$ -specific mouse monoclonal antibody to each well. The plate was then sealed and incubated overnight at 4 °C. After washing the plate four times with washing buffer [0.05% phosphate-buffered saline with Tween<sup>®</sup> 20 (PBST, Sigma-Aldrich, St Louis, MO, USA)], 200  $\mu$ L 1 $\times$  Assay Diluent A solution was then added to each well for 1 h at room temperature for blocking. Standard dilutions and samples (100  $\mu$ L) with measured concentrations were separately added to the appropriate wells for 2 h to ensure that the samples were bound to the immobilized capture antibody. Subsequently, 100  $\mu$ L of biotinylated goat polyclonal anti-human interleukin (IL)-1 $\beta$  detection antibody was added to each well for 1 h, producing an antibody-antigen-antibody 'sandwich'. Avidin-horseradish peroxidase (HRP) was then added for 30 min, followed by Substrate Solution F for 10 min, producing a blue colour in proportion to the concentration of IL-1 $\beta$  present in the sample. Finally, the stop solution (2N H<sub>2</sub>SO<sub>4</sub>) was added to change the reaction colour from blue to yellow, and the microwell absorbance was read at 450 nm using a microplate reader (Bio-Rad 680 Microplate reader, Hercules, CA, USA). The plate was washed four times with 0.05% PBST solution between each step, except following primary antibody coating. All procedures were implemented at room temperature.

### Immunohistochemistry

All tissue specimens (PGs, RCs and normal pulp tissues) were fixed in 10% neutral-buffered formalin solution for 24 h before being embedded in paraffin. The 2- $\mu$ m-thick serial paraffin section slides were dewaxed in xylene and rehydrated using a graded ethanol series. For antigen retrieval, tissue sections for analysis of HIF-1 $\alpha$ , BECN1, Atg5-12 and LC3 were placed in 0.01 mol L<sup>-1</sup> citrate buffer solution (Dako target retrieval solution, pH 9; Dako, Glostrup, Denmark) and heated separately (1000 W) for 15 min in a microwave. Tissue sections for analysis of BNIP3 and pAMPK were immersed in Ventana<sup>®</sup> Cell Conditioning Solution-1 (Cat. No. 760-700; Ventana, Tucson, AZ, USA) for 32 min, following which 3% hydrogen peroxide was used to block endogenous peroxidase activity in all tissue sections. The sections used for HIF-1 $\alpha$ , BECN1, Atg5-12 and LC3 analysis were incubated with rabbit primary antibodies [HIF-1 $\alpha$  (Abcam, Cambridge, UK; Cat. No. ab51608; 1 : 50); BECN1 (Santa Cruz, Dallas, Texas, USA, Cat. No. sc-11427; 1 : 50); Atg5-12: (Abcam, Cat. No.

ab155589; 1 : 100); LC3 (Abcam, Cat. No. ab52768; 1 : 800)] for 30 min at 37 °C and then incubated with Super Enhancer<sup>™</sup> Reagent (BioGenex, Fremont, CA, USA; Cat. No. QD430-XAKE) for 20 min, followed by Poly HRP Reagent (BioGenex) for 20 min. Subsequently, the sections were treated with 3,3'-diaminobenzidine (DAB, Roche, Indianapolis, IN, USA; Cat. No. 1718096) for 8 min. Between each step, the sections were washed three times with Tris-buffered saline (TBS) solution (Sigma-Aldrich).

On the other hand, the sections for BNIP3 and pAMPK analysis were incubated with rabbit primary antibodies [BNIP3 (Abcam, Cat. No. ab38621; 1 : 50); pAMPK (Santa Cruz, Dallas, TX, USA, Cat. No. sc-101630; 1 : 50)] for 30 min, followed by the secondary antibody with OptiView<sup>®</sup> HQ Universal Linker (Ventana) for 8 min, then HRP multimers (Ventana) for another 8 min at room temperature. Subsequently, all sections were treated with DAB (Roche) reagent for 8 min, followed by OptiView<sup>®</sup> Copper for 4 min, the sections being washed with Ventana<sup>®</sup> reaction buffer (Ventana) three times between each step.

Finally, all sections were counterstained with Mayer's haematoxylin and then mounted. IHC staining was evaluated under a light microscope. Each set of experiments included a positive control, which were followed aforementioned procedures of immunostaining to ensure the reproducibility of the staining process. The tissues of positive controls (human breast carcinoma tissues) were employed according to the datasheets of the manufacturers for each antibody (human breast carcinoma tissues for HIF-1 $\alpha$ , pAMPK, BNIP3, BECN1, Atg5-12 and LC3). Negative controls (human adipose tissues) were included by following the same procedure.

Quantification and analysis of the stained IHC slides (cytoplasm or nuclei) were performed by the first author and the corresponding author with mutual discussion using the semi-automated image analysis software Image J Version 1.51e. The entire stained slides were observed with different magnifications (40-, 100- 200-fold) to determine cell type and pattern of positive staining microscopically. Then, for quantification of positive staining, ten views of every immunostained sections were randomly selected under 200-fold magnification. The score of the percentage of positive IHC staining (*P*) was classified as follows: 0 (0-4%), 1 (5-24%), 2 (25-49%), 3 (50-74%) and 4 (75-100%), whereas the score for the intensity of staining (*I*) was classified as 0, no

staining; 1, light yellow colour (weak staining); 2, brown colour (moderate staining); and 3, dark brown colour (strong staining). The total score (S) was then calculated as  $P \times I$  for each section (Sarbia et al. 1999).

### Western blot

Proteins were extracted from each of the samples from PG, RC and normal pulp tissue. Total protein was measured using a protein assay dye (Bio-Rad). An average amount (50 µg) of proteins was placed into 5× loading buffer [ $\beta$ -mercaptoethanol, 55 mmol L<sup>-1</sup> (Gibco, Glen Burnie, MD, USA; Cat. No. 21985023), bromophenol blue (Bio-RAD, Cat. No. 1610404)]. The protein was then denatured by boiling in 95 °C water for 5 min. After cooling, the samples were subjected to sodium dodecyl sulphate polyacrylamide gel electrophoresis (SDS-PAGE) (gel obtained from Bio-Rad) at 100 V for 30 min, followed by 125 V for a further 50 min, and the reaction was then stopped when all the protein markers (PageRuler™ prestained Protein ladder; Fermentas, Glen Burnie, MD, USA) were noted to be at the bottom of the gel.

The gel was gently removed and transferred onto a polyvinylidene difluoride (PVDF) membrane (Millipore, Billerica, MA, USA). A semi-dry transfer machine (Trans-Blot® SD Semi-Dry Transfer Cell) was used to transfer the proteins (0.2 A, 10 V for 2 h). Subsequently, the membranes were blocked with 5% bovine serum albumin (BSA) in phosphate-buffered saline (PBS) solution at room temperature for 1 h and incubated overnight at 4 °C with the following primary antibodies (each at a dilution of 1 : 1000): pAMPK (Cell Signaling, Boston, MA, USA; Cat. No. 2537), HIF-1 $\alpha$  (Cell Signaling, Cat. No. 3716), BNIP3 (Cell Signaling, Cat. No. 13795), BECN1 (Santa Cruz, Cat. No. sc-11427), Atg5-12 (Cell Signaling, Cat. No. 2010), LC3 (Abgent, San Diego, CA, USA; Cat. No. AP1802a), p62 (Santa Cruz, Cat. No. sc-28359) and  $\beta$ -actin (Millipore, Cat. No. MAB1501; 1 : 5000). The blots were then incubated with diluted HRP-conjugated secondary antibody (1 : 5000) for 1 h with gentle agitation at room temperature. Between steps, the membrane was washed with 0.1% PBST for 5 min 3 times.

For visualization of protein bands, a chemiluminescent HRP (ECL) system (Immobilon Western Chemiluminescent HRP Substrate; Millipore, Cat. No. WBKLS0500) was used. The HRP substrate consisted of equal volumes of luminol reagent and peroxide solution. The blot was placed side-up in a clean

container containing HRP substrate for 1 min at room temperature. The blot was subsequently exposed in a chemiluminescent imaging analyzer (BioSpectrum® 800 Imaging System, Upland, CA, USA) six times for an exposure duration of 30 s, and images captured using a high-resolution charge-coupled device (CCD) camera were stored in Joint Photographic Experts Group (JPEG) format. The amount of protein was then quantified using a Fuji LAS-4000 lumino image analyzer (Fuji Photo Film Co., Tokyo, Japan). The ratio was evaluated as normalized by the  $\beta$ -actin signal.

### Transmission electron microscopy

After immediate fixation of the dissected tissue samples of inflamed periapical lesions (PGs, and RCs) ( $2 \times 2$  mm<sup>2</sup>) in 2.5% glutaraldehyde solution, the samples were stored overnight at 4 °C. They were then washed briefly with 200 mmol L<sup>-1</sup> cacodylate buffer (pH 7.0), post-fixed with 1% osmium tetroxide for 1 h at 4 °C and dehydrated through a series of acetones and propylene oxide, before being embedded in Spurr epoxy resin (Polysciences, Warrington, PA, USA). Heavy metal stain and an ultramicrotome (Leica EM UC7, Buffalo Grove, IL, USA) were applied to the ultrathin sections of 70–90 nm in thickness, which were then mounted on copper or nickel grids and further dried in a desiccator or under vacuum for 2 h. The tissue sections were contrasted with uranyl acetate and lead citrate and then examined using a Hitachi HT-7700 transmission electron microscope operating at 120 kV (Hitachi, Tokyo, Japan).

### Statistical analyses

All statistical analyses were performed using SPSS software (version 20.0, SPSS Inc, Chicago, IL, USA). Non-parametric Kruskal–Wallis tests were used for analysis of different types of samples. Two-sample comparisons were assessed using the Mann–Whitney *U*-test. Statistical significance was considered when *P* value < 0.05.

## Results

### A significantly high interleukin (IL)-1 $\beta$ expression in periapical lesions

The concentration of cytokine IL-1 $\beta$ , as measured by ELISA, indicated the degree of inflammation. The concentrations of IL-1 $\beta$  in PGs and RCs were significantly increased as compared to normal pulp tissues

( $P < 0.05$ ). On the other hand, the concentration of IL-1 $\beta$  in PGs was higher than that in RCs, but there was no significant difference ( $P = 0.372$ ; Fig. 1).

### Highly-expressed immunostainings of hypoxia-related (HIF-1 $\alpha$ , pAMPK and BNIP3) and autophagy-related (BECN1, Atg5–12) proteins in periapical lesions

The intensity and pattern of immunostaining of hypoxia-related (HIF-1 $\alpha$ , pAMPK, and BNIP3) (Fig. 2a-i) and autophagy-related proteins (BECN1, Atg5–12, and LC3) (Fig. 3a-i) in RCs, PGs and normal pulp tissues are summarized in Table 3. Stronger cytoplasmic staining of pAMPK, HIF-1 $\alpha$ , BECN1, Atg5–12 and BNIP3 proteins and more intensive nuclear staining of HIF-1 $\alpha$  and BECN1 proteins were observed in all samples of PGs and RCs as compared to normal pulp tissues. In contrast, the cytoplasmic staining of LC3 protein was weaker in both PGs and RCs as compared to normal pulp tissues. In both types of periapical lesion, the cytoplasmic/nuclear staining was strongly expressed in inflammatory cells (macrophages, lymphocytes and PMNs), endothelial cells and fibroblasts. In addition, positive staining in all layers of the epithelial lining of RCs was observed for each specimen, as well as in inflammatory cells within the cystic capsule. On the other hand, in the samples of normal pulp tissues, positive staining of HIF-1 $\alpha$ , pAMPK, BNIP3, BECN1, Atg5–12 and LC3 proteins was observed in fibroblasts and endothelial cells.

Positive staining were noted for the positive control tissues whilst negative staining were observed for the negative control tissues for each of the antibodies (Figures S1 and S2).

Regarding the immunoscores, statistically significant increases in pAMPK, HIF-1 $\alpha$ , BNIP3 and Atg5–12 proteins ( $P < 0.005$ ) were observed in inflammatory periapical lesions (PGs and RCs) as compared to normal pulp tissues, whilst there were no significant differences between PGs and RCs ( $P > 0.05$ ). In contrast, significantly lower immunoscores of LC3 protein were noted in both types of periapical lesion as compared to normal pulp tissues ( $P < 0.0001$ ); however, positive staining was still observed in the cytoplasm of inflammatory cells, endothelial cells and all layers of the epithelial lining of RCs. On the other hand, the immunoscores of BECN1 protein were similar in PGs, RCs ( $P > 0.05$ ), but a little higher in RCs when compared to normal pulp tissue ( $P = 0.03$ ; Table 3; Fig. 4).

### Highly-expressed immunoblottings of hypoxia-related (pAMPK, HIF-1 $\alpha$ and BNIP3) and autophagy-related (Atg5–12, and LC3II) proteins and ratios of LC3II/LC3I in periapical lesions, whilst low expressed of p62 was detected

The expressions of hypoxia-related proteins (pAMPK, HIF-1 $\alpha$  and BNIP3) and autophagy-related proteins (BECN1, Atg5–12, LC3I, LC3II and p62) in periapical lesions (PGs and RCs) and normal pulp tissues were demonstrated by WB analysis (Fig. 5). The

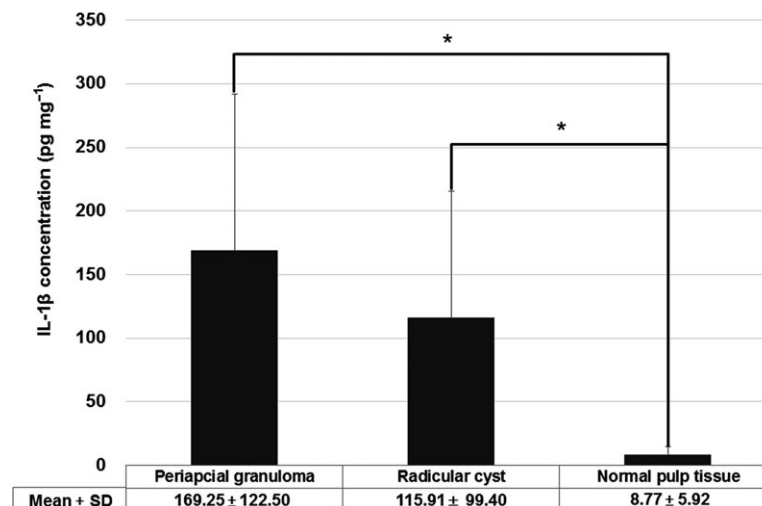


**Figure 1** ELISA assay of IL-1 $\beta$  concentration in periapical granulomas (PGs), radicular cysts (RCs) and normal pulp tissue. The concentrations of IL-1 $\beta$  in PGs and RCs were significantly increased as compared with normal pulp tissue ( $*P < 0.05$ ).

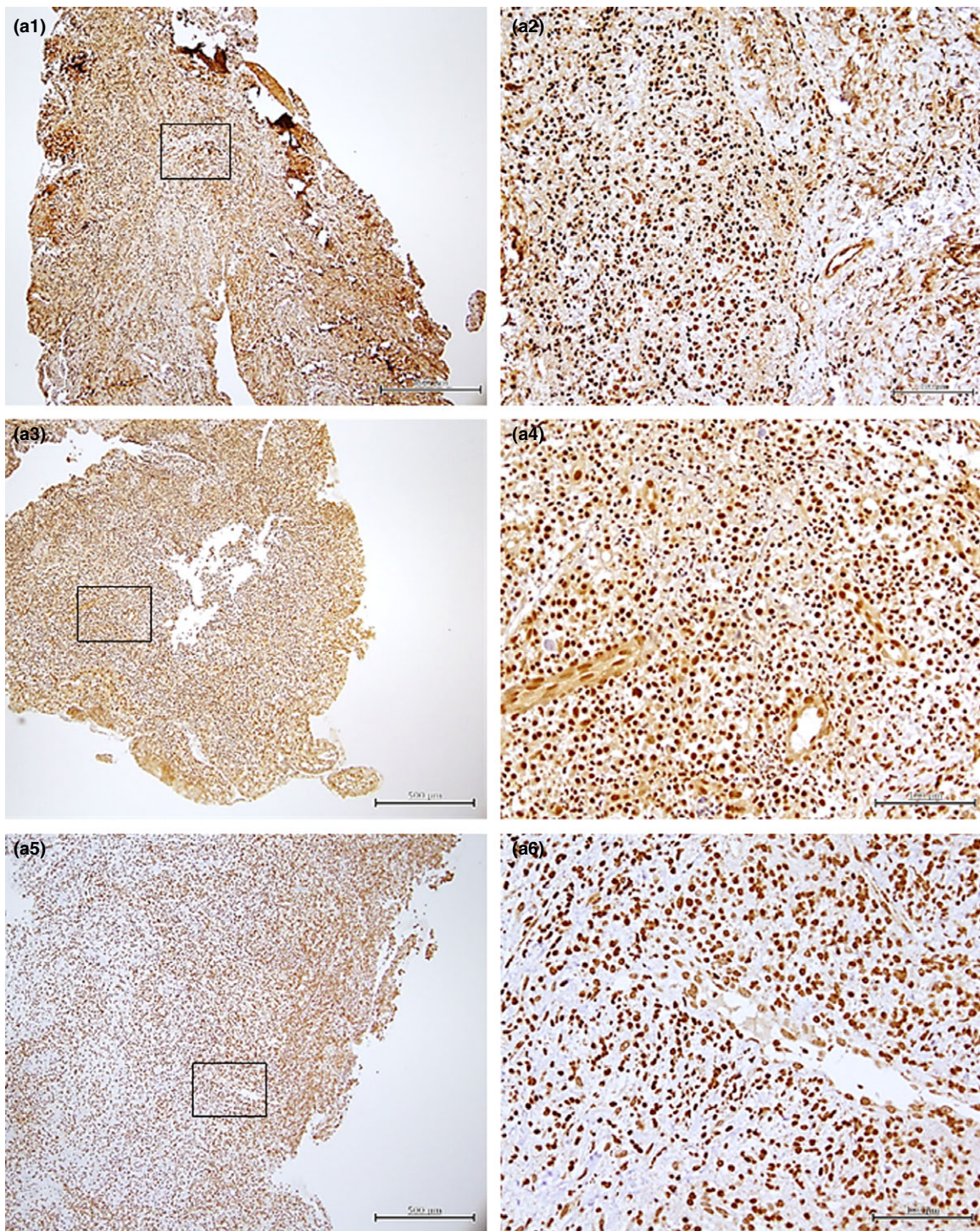


**Figure 2** Representative immunostainings of hypoxia-related proteins (HIF-1 $\alpha$ , pAMPK and BNIP3). HIF-1 $\alpha$ : periapical granuloma (a1, a2), radicular cyst (b1, b2), normal pulp tissue (c1, c2); pAMPK: periapical granuloma (a3, a4), radicular cyst (b3, b4), normal pulp tissue (c3, c4); BNIP3: periapical granuloma (a5, a6), radicular cyst (b5, b6), normal pulp tissue (c5, c6) (magnification: a1, b1, c1, a3, b3, c3, a5, b5, c5  $\times$ 40; a2, b2, c2, a4, b4, c4, a6, b6, c6  $\times$ 200). Scale bars of  $\times$ 40 = 500  $\mu$ m; scale bars of  $\times$ 200 = 100  $\mu$ m.

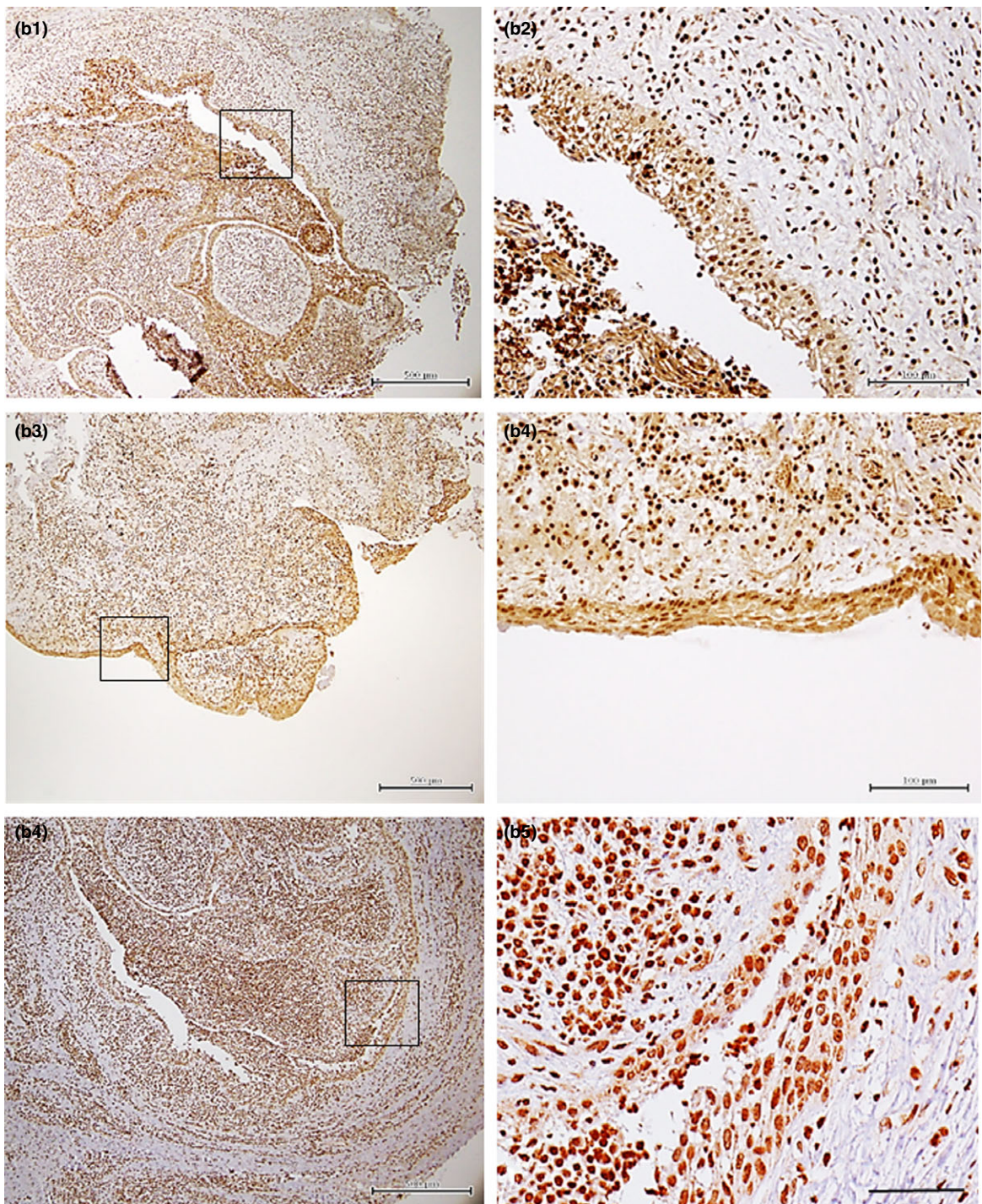


**Figure 2** Continued.

expressions of hypoxia-related proteins (pAMPK, HIF-1 $\alpha$  and BNIP3) and autophagy-related proteins (Atg5–12 and LC3 II) were significantly higher

( $P < 0.001$ ) in PG and RC than in the normal pulp tissues, the exceptions being LC3I and p62 proteins (Fig. 6).

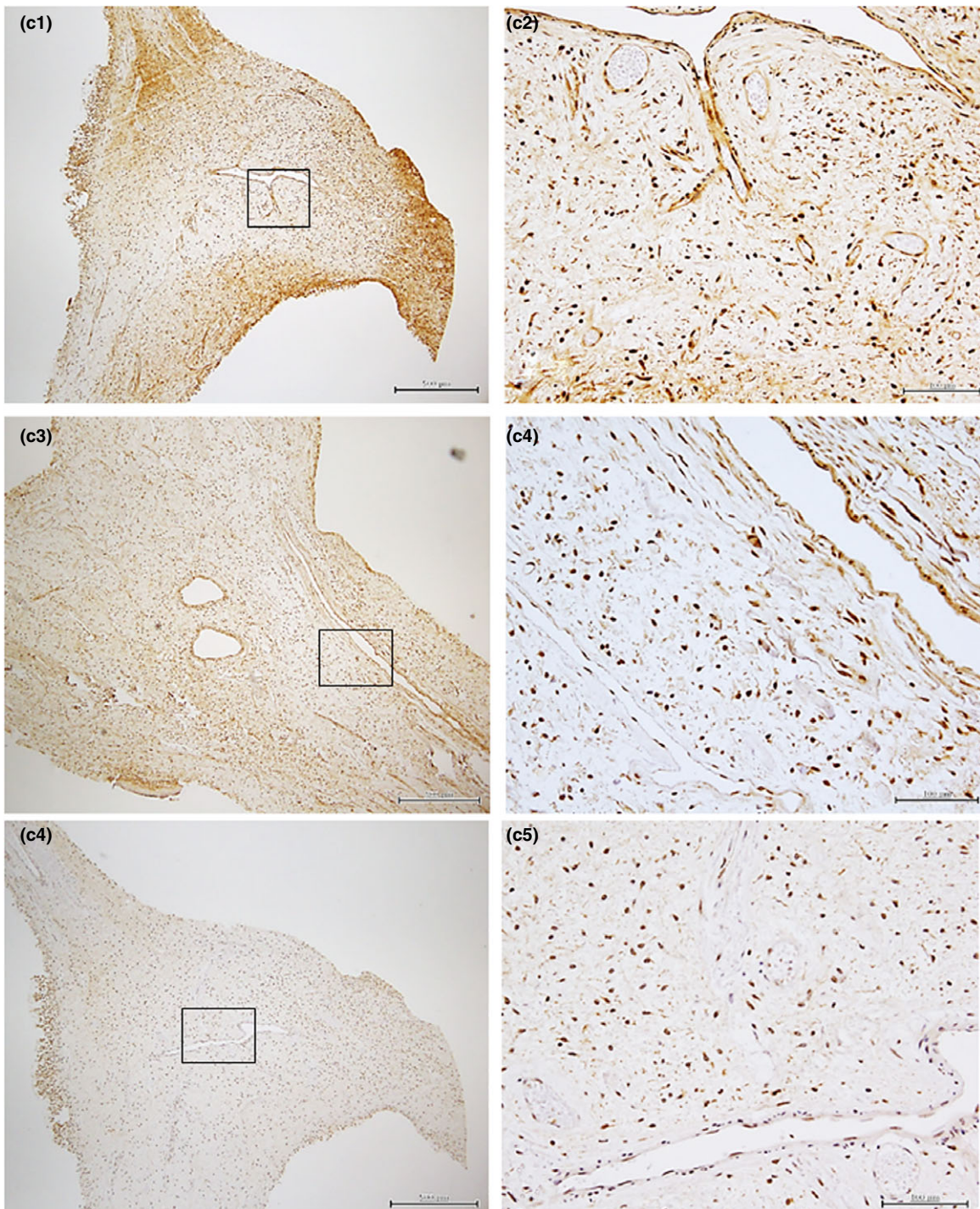


**Figure 2** Continued.

For the hypoxia-related proteins (pAMPK, HIF-1 $\alpha$  and BNIP3), the expressions of pAMPK and BNIP3 proteins in the periapical lesions (PGs and RCs) were

significantly higher ( $P < 0.01$ ) than in normal pulp tissues. HIF-1 $\alpha$  showed a significantly higher ( $P < 0.01$ ) expression only in PGs as compared to

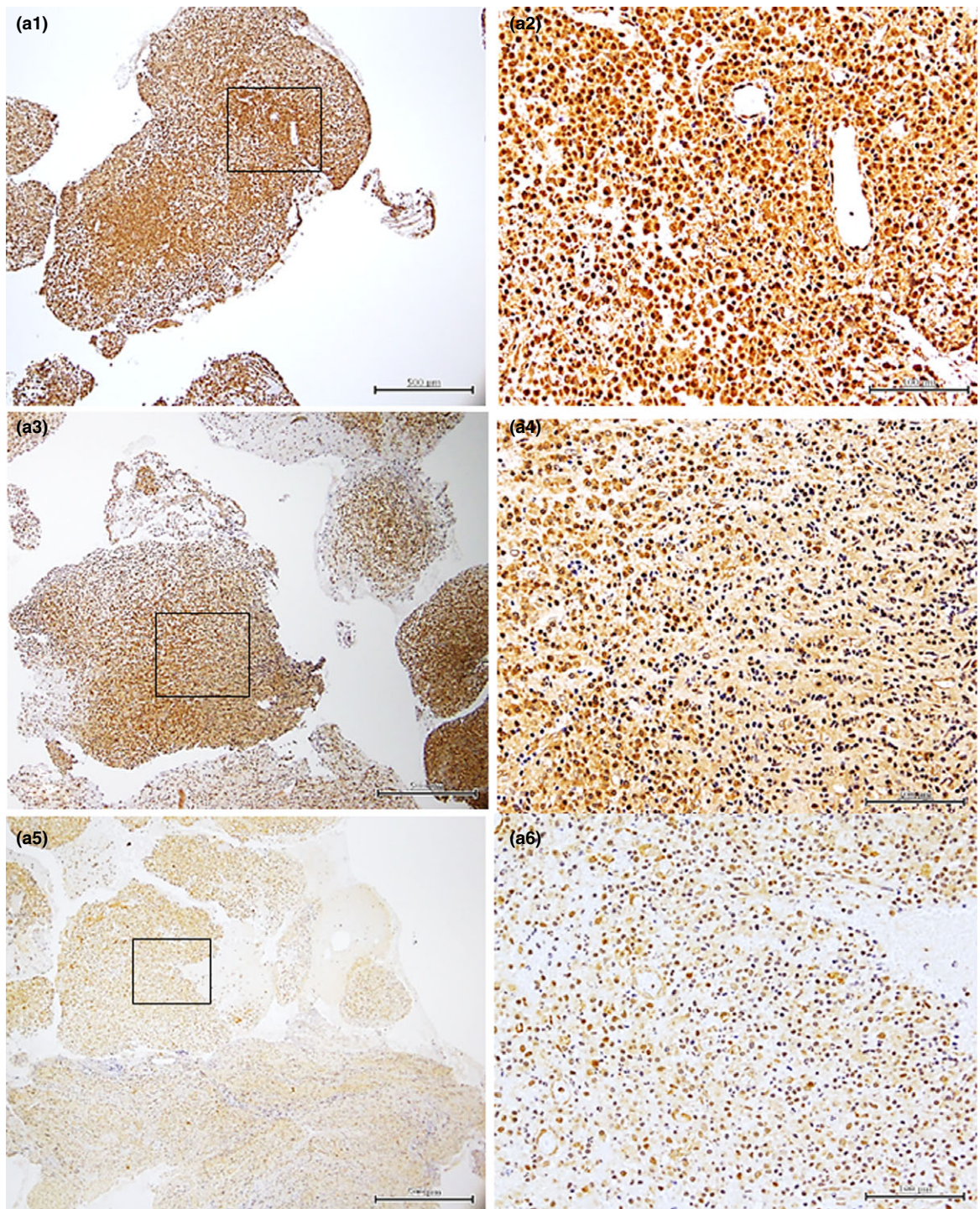


**Figure 3** Representative immunostaining of autophagy-related proteins (BECN1, Atg5–12 and LC3). BECN1: periapical granuloma (a1, a2), radicular cyst (b1, b2), normal pulp tissue (c1, c2); Atg5–12: periapical granuloma (a3, a4), radicular cyst (b3, b4), normal pulp tissue (c3, c4); LC3: periapical granuloma (a5, a6), radicular cyst (b5, b6), normal pulp tissue (c5, c6) (magnification: a1, b1, c1, a3, b3, c3, a5, b5, c5  $\times$  40; a2, b2, c2, a4, b4, c4, a6, b6, c6  $\times$  200). Scale bars of  $\times$  40 = 500  $\mu$ m; scale bars of  $\times$  200 = 100  $\mu$ m.

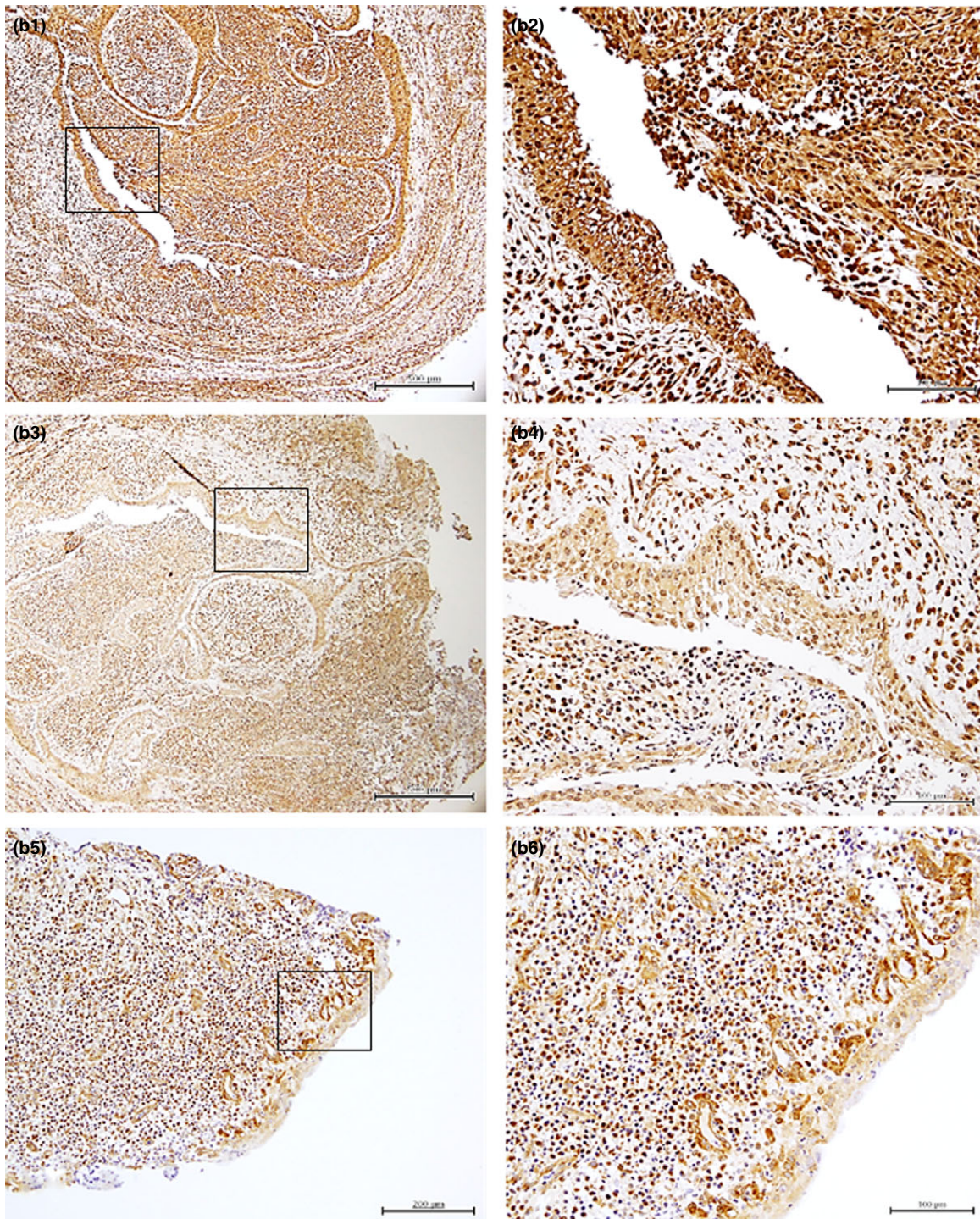


**Figure 3** Continued.

normal pulp tissues. However, pAMPK demonstrated a significantly higher ( $P < 0.05$ ) expression than HIF-1 $\alpha$  in both PGs and RCs (Fig. 6).

For the autophagy-related proteins (BECN1, Atg5-12, LC3I, LC3II and p62), there were significant differences ( $P < 0.05$ ) in Atg5-12, LC3I, LC3II and p62

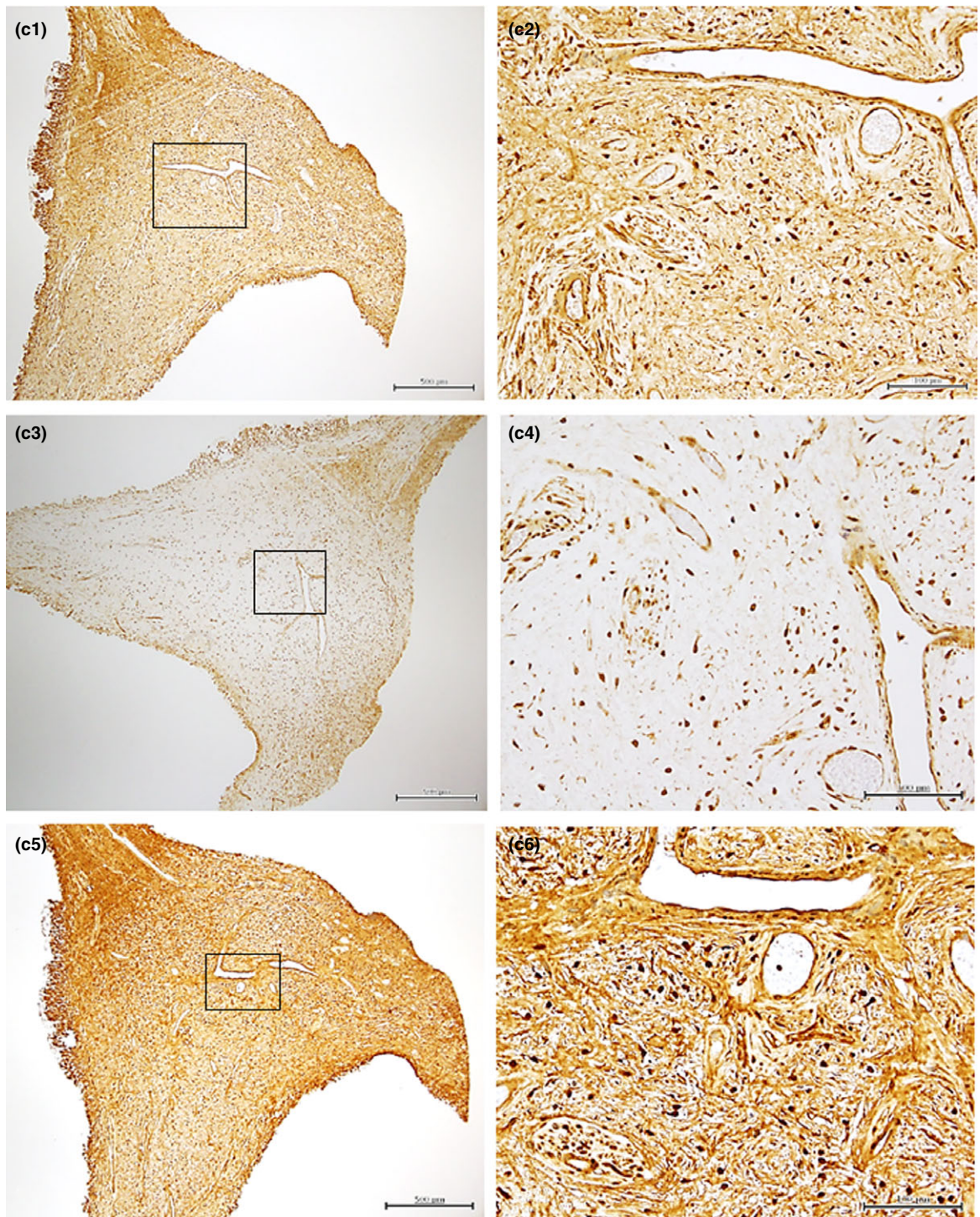


**Figure 3** Continued.

protein expressions between the PGs, RCs and normal pulp tissues. Higher expressions ( $P < 0.05$ ) of Atg5–12 and LC3II proteins were found in PGs and RCs

than in normal pulp tissues. Although the LC3I expression was significantly lower ( $P < 0.001$ ) in both periapical lesions than in normal pulp tissue, the

**Table 3** Summary of the characteristics of immunostaining of hypoxia-related (HIF-1 $\alpha$ , pAMPK, and BNIP3) and autophagy-related proteins (BECN1, Atg5–12 and LC3) in periapical granuloma (PG), radicular cyst (RC) and normal pulp tissue (NP)

	PG	RC	NP
<b>Hypoxia-related proteins</b>			
<b>HIF-1<math>\alpha</math></b>			
Intensity and pattern	C (2), N (2) IC, EC, FB	C (2), N (2) CL, IC, EC, FB	C (1), N (1) EC, FB
Percentage (%) (mean $\pm$ SD)	62 $\pm$ 23	59 $\pm$ 24	23 $\pm$ 9
Total scores <sup>†</sup> (mean $\pm$ SD)	8.2 $\pm$ 3.0	7.8 $\pm$ 3.6	3.3 $\pm$ 1.0
<i>P</i> value	PG vs. RC: 0.8; PG vs. NP: <0.0001*	RC vs. NP: 0.001*	
<b>pAMPK</b>			
Intensity and pattern	C (2), N (2) IC, EC, FB	C (2), N (2) CL, IC, EC, FB	C (1), N (1) EC, FB
Percentage (%) (mean $\pm$ SD)	74 $\pm$ 18	81 $\pm$ 8	20 $\pm$ 9
Total scores <sup>†</sup> (mean $\pm$ SD)	9.9 $\pm$ 2.9	10.5 $\pm$ 2.3	2.5 $\pm$ 1.0
<i>P</i> value	PG vs. RC: 0.68; PG vs. NP: <0.0001*	RC vs. NP: <0.0001*	
<b>BNIP3</b>			
Intensity and pattern	C (2), N (2) IC, EC, FB	C (2), N (1) CL, IC, EC, FB	C (1), N (0) EC, FB
Percentage (%) (mean $\pm$ SD)	56 $\pm$ 30	58 $\pm$ 24	26 $\pm$ 13
Total scores <sup>†</sup> (mean $\pm$ SD)	5.9 $\pm$ 3.3	5.8 $\pm$ 2.8	2.7 $\pm$ 1.3
<i>P</i> value	PG vs. RC: 0.95; PG vs. NP: 0.004*	RC vs. NP: 0.002*	
<b>Autophagy-related proteins</b>			
<b>BECN1</b>			
Intensity and pattern	C (2), N (2) IC, EC, FB	C (2), N (1) CL, IC, EC, FB	C (2), N (1) EC, FB
Percentage (%) (mean $\pm$ SD)	75 $\pm$ 22	81 $\pm$ 15	72 $\pm$ 6
Total scores <sup>†</sup> (mean $\pm$ SD)	8.8 $\pm$ 3.0	9.9 $\pm$ 2.4	7.9 $\pm$ 1.4
<i>P</i> value	PG vs. RC: 0.26; PG vs. NP: 0.376	RC vs. NP: 0.03*	
<b>Atg5–12</b>			
Intensity and pattern	C (2), N (0) IC, EC, FB	C (2), N (0) CL, IC, EC, FB	C (1), N (0) EC, FB
Percentage (%) (mean $\pm$ SD)	53 $\pm$ 21	62 $\pm$ 23	36 $\pm$ 16
Total scores <sup>†</sup> (mean $\pm$ SD)	5.6 $\pm$ 2.8	6.8 $\pm$ 3.2	2.5 $\pm$ 0.9
<i>P</i> value	PG vs. RC: 0.28; PG vs. NP: 0.001*	RC vs. NP: <0.0001*	
<b>LC3</b>			
Intensity and pattern	C (1), N (0) IC, EC, FB	C (1), N (0) CL, IC, EC, FB	C (2), N (0) EC, FB
Percentage (%) (mean $\pm$ SD)	53 $\pm$ 25	56 $\pm$ 20	76 $\pm$ 14
Total scores <sup>†</sup> (mean $\pm$ SD)	4.3 $\pm$ 2.1	5.2 $\pm$ 1.9	8.6 $\pm$ 2.5
<i>P</i> value	PG vs. RC: 0.17; PG vs. NP: <0.0001*	RC vs. NP: <0.0001*	

Values in parentheses indicate intensity of staining: (0) negative; (1) weakly positive; (2) moderately positive; (3) strongly positive.

\*Significant difference,  $P < 0.05$ .

<sup>†</sup>Total scores = intensity  $\times$  percentage of each sample.

C, cytoplasm; N, nuclear; SD, standard deviation; CL, cystic lining; IC, inflammatory cells; EC, endothelial cells; FB, fibroblasts.

ratio of LC3II/LC3I in normal pulp tissue was far below one (LC3II/LC3I = 0.06), and this was reversed in periapical lesions (LC3II/LC3I in PGs = 1.16; LC3II/LC3I in RCs = 1.24) (Fig. 7). On the other hand, the expression of p62 protein was significantly lower ( $P < 0.001$ ) in both periapical lesions (PGs and RCs) than in normal pulp tissue (Fig. 6).

Additionally, comparing the expressions of the autophagy-related and hypoxia-related proteins with the size of the periapical lesions detected on periapical

radiographic examination, increased expressions of pAMPK, BNIP3, BECN1, LC3I, LC3II and p62 proteins were observed in the sample of lesions of a size  $>10^2$  mm<sup>2</sup> as compared to the sample of lesions of  $\leq 10^2$  mm<sup>2</sup>. On the other hand, pAMPK expression was slightly higher without significant difference ( $P = 0.16$ ) in the periapical lesions of a size  $>10^2$  mm<sup>2</sup>. In contrast, an increased HIF-1 $\alpha$  expression in the periapical lesions  $\leq 10^2$  mm<sup>2</sup> in size was noted but there was no significant difference ( $P = 0.53$ ) (Fig. 8).

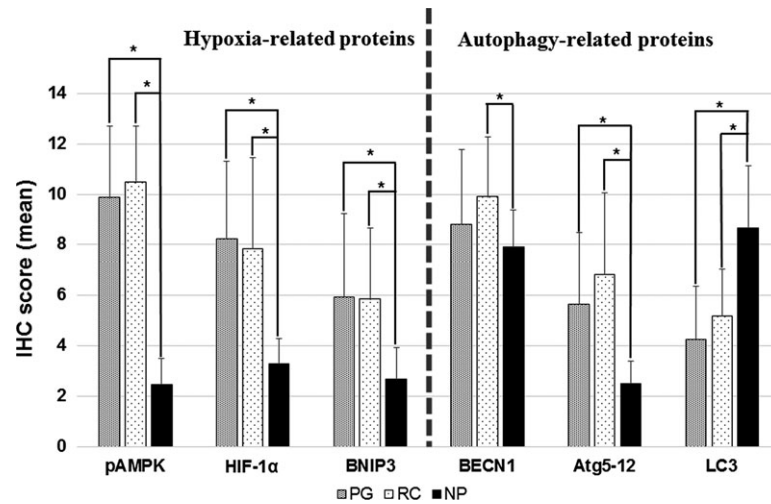


**Figure 4** Quantitative analyses of immunoscores of hypoxia-related (pAMPK, HIF-1 $\alpha$  and BNIP3) and autophagy-related proteins (BECN1, Atg5-12 and LC3) for radicular cysts (RCs), periapical granulomas (PGs) and normal pulp tissue (NP) on immunohistochemical staining (bars represent mean  $\pm$  standard deviation of the mean; \* $P$  < 0.05 compared with normal pulp tissue).

#### Unique ultrastructure of autophagosomes/autolysosomes in inflamed periapical lesions

TEM was used to further confirm the presence of an ultrastructure of autophagosomes in inflamed periapical lesions examined in the study. Autophagosomes and autolysosomes consisted of a double-membrane structure containing cytoplasmic components were detected in PGs (Fig. 9) and RCs (Fig. 10).

#### Discussion

Three different kinds of tissue samples (PGs, RCs and normal pulp tissue) were recruited in the study; the inflammatory degree was detected first using ELISA whilst IHC and WB analyses were then employed to identify the expressions of hypoxia-related (HIF-1 $\alpha$ , BNIP3 and pAMPK) and autophagy-related proteins (BECN-1, Atg5-12, LC3 and p62), TEM was used to explore the ultrastructural morphology of autophagy in human inflamed periapical lesions (PGs and RCs).

It is widely accepted that RCs and PGs are derived from inflamed periapical tissues characterized by infiltration of lymphocytes, plasma cells and macrophages (Lin *et al.* 2009). Various cytokines, including IL-1 ( $\alpha$ , and  $\beta$ ), IL-6, TNF $\alpha$  and MMP-9, are elicited by immune and inflammatory cells. RCs and PGs have been reported to exhibit positive immunostaining for IL-1 ( $\alpha$  and  $\beta$ ) and IL-6 located in epithelial cells and in endothelial cells of blood vessels (Bando *et al.*

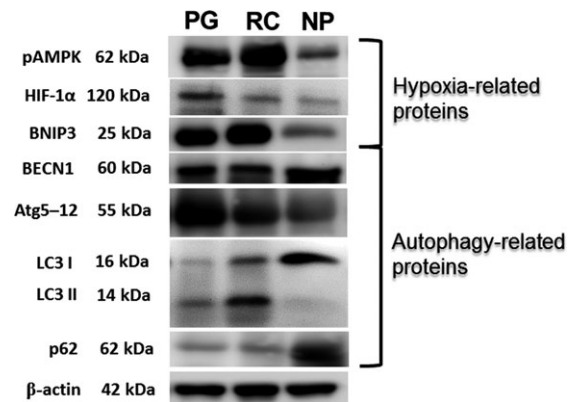


**Figure 5** Representative immunoblots of hypoxia-related (pAMPK, HIF-1 $\alpha$  and BNIP3) and autophagy-related proteins (BECN1, Atg5-12, LC3I, LC3II and p62) for periapical granulomas (PGs), radicular cysts (RCs) and normal pulp tissues (NP).

1993). Moreover, ELISA showed that IL-1 $\beta$  was only found in inflammatory RCs and not in other developmental cysts (e.g. odontogenic keratocysts (now named keratocystic odontogenic tumours) and follicular cysts) (Meghji *et al.* 1996). Increased expression of IL-1 $\beta$  may also be associated with the development of periapical lesions (Dill *et al.* 2015). Pathogen-elicited inflammatory responses not only normally occur in hypoxic microenvironments (Dehne & Brüne 2009), but also enhance the expression of hypoxic proteins by secreting a variety of cytokines from inflamed,

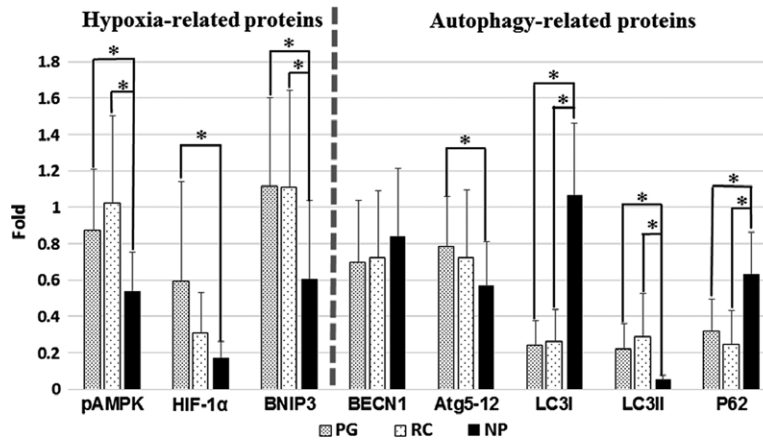


**Figure 6** Quantitative analyses of Western blots of hypoxia-related (pAMPK, HIF-1α and BNIP3) and autophagy-related proteins (BECN1, Atg5-12, LC3I, LC3II and p62) for radicular cysts (RCs), periapical granulomas (PGs) and normal pulp tissue (NP). The results were quantified using densitometric analysis and normalized by the level of β-actin (bars represent mean ± standard deviation of the mean; \*P < 0.05 compared with normal pulp tissue).

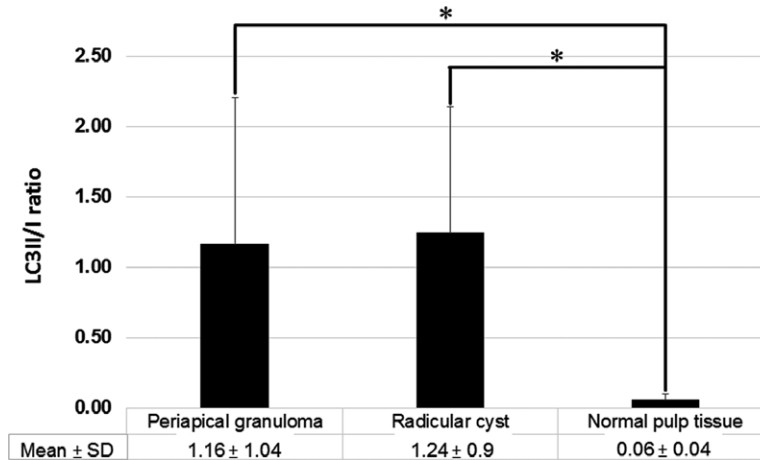


**Figure 7** Ratios of LC3II/LC3I in radicular cysts, periapical granulomas and normal pulp tissue. The ratio of LC3II/LC3I in normal pulp tissue was significantly lower than the ratios in radicular cysts and periapical granulomas (bars represent mean ± standard deviation of the mean; \*P < 0.05 compared with normal pulp tissue).

infiltrating immune cells and stromal cells (Westra *et al.* 2007). Importantly, hypoxia even stimulates proinflammatory cytokines in macrophages and endothelial cells (Moreau *et al.* 2005). Thus, taken together, the ELISA results demonstrating an increased IL-1β concentration in RCs and PGs as compared to normal pulp tissue in the current study indicated the inflammatory status of the periapical lesions (RCs and PGs) and may also imply the existence of hypoxic microenvironments in these periapical lesions.

Due to ischaemia and nutritional deficiency, hypoxia is an environment speculated to exist in the

centre of inflammatory periapical lesions (Lin *et al.* 2009). It is worthwhile to examine whether hypoxia-related proteins HIF-1α, pAMPK and BNIP3 are expressed in periapical lesions (PGs and RCs) and normal pulp tissue. In the present study, strong immunostainings of HIF-1α, pAMPK and BNIP3 were demonstrated in all samples of periapical lesions, whilst only weak immunostaining was found in normal pulp tissue. Additionally, positive immunostainings were present in inflammatory cells (plasma cells and macrophages) and fibroblasts, as well as in the epithelial layers of RCs, suggesting that the presence of HIF-1α, pAMPK and BNIP3 is a result of localized

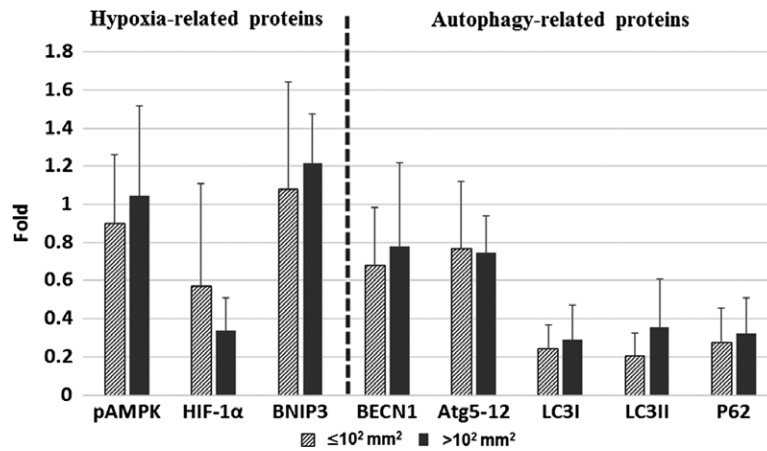


**Figure 8** Relationships of the expressions of hypoxia-related and autophagy-related proteins with lesion size, as assessed by comparison of two groups of lesions, the first consisting of lesions  $\leq 10^2$  mm<sup>2</sup>, the second of lesions  $>10^2$  mm<sup>2</sup> in size, as assessed by periapical radiographic examination (bars represent mean  $\pm$  standard deviation of the mean).

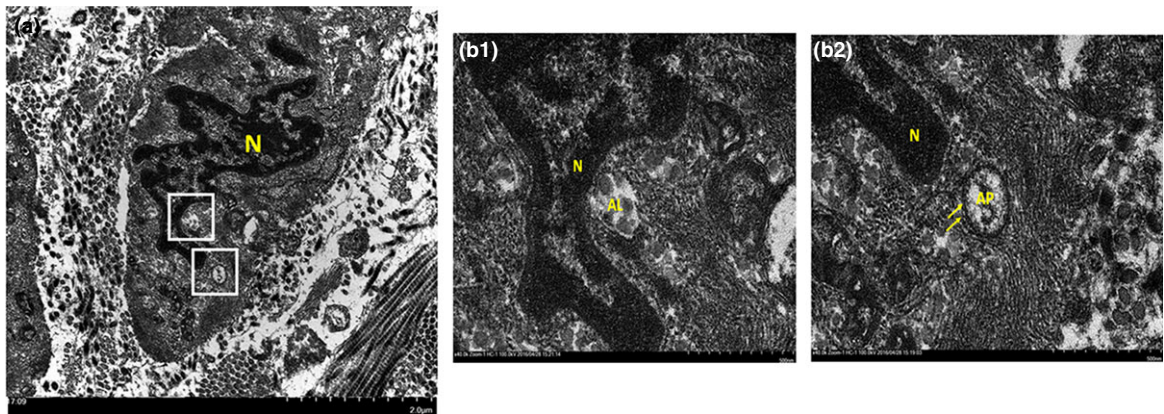


**Figure 9** (a) Representative ultrastructural morphology of autophagy in a periapical granuloma by transmission electron microscopy (N: nucleus;  $\times 8000$ ); (b1, b2) double-membrane vacuoles (yellow arrows) were observed in the areas denoted by white squares in (a) (AP: autophagosome; AL: autolysosome;  $\times 40,000$ ).

hypoxia and energy depletion due to ischaemia during cystic and granuloma development. Moreover, the finding of HIF-1 $\alpha$  in the present study was compatible with previously reported findings in human and rat polycystic kidneys (Bernhardt *et al.* 2007).

Additionally, the pattern of hypoxia in the current study demonstrated by IHC staining was compatible with the results of WB analysis. In the WB analyses, significantly higher expressions of pAMPK and BNIP3 proteins in periapical lesions were noted (PGs and RCs) as compared to normal pulp tissues. HIF-1 $\alpha$  was also more highly expressed in PGs and RCs than in normal pulp tissues; however, a significant difference only existed between PGs and normal pulp tissue. On

the other hand, pAMPK demonstrated a significantly higher expression than HIF-1 $\alpha$  in both PGs and RCs (Fig. 6).

It is well-known that autophagy plays a key role in adaption to nutrient depletion and hypoxia and confers protection to increase cell survival (Kamada *et al.* 2004, Eskelinen 2005, Rubinsztein *et al.* 2011). Thus, the present findings implied that hypoxia-related proteins could induce autophagy in periapical lesions associated with the pAMPK/mTOR or HIF-1 $\alpha$ /BNIP3 signalling pathways, and pAMPK might be the predominant pathway, as it has been found that pAMPK exhibited a significantly higher expression than HIF-1 $\alpha$  in both PGs and RCs. Furthermore, the

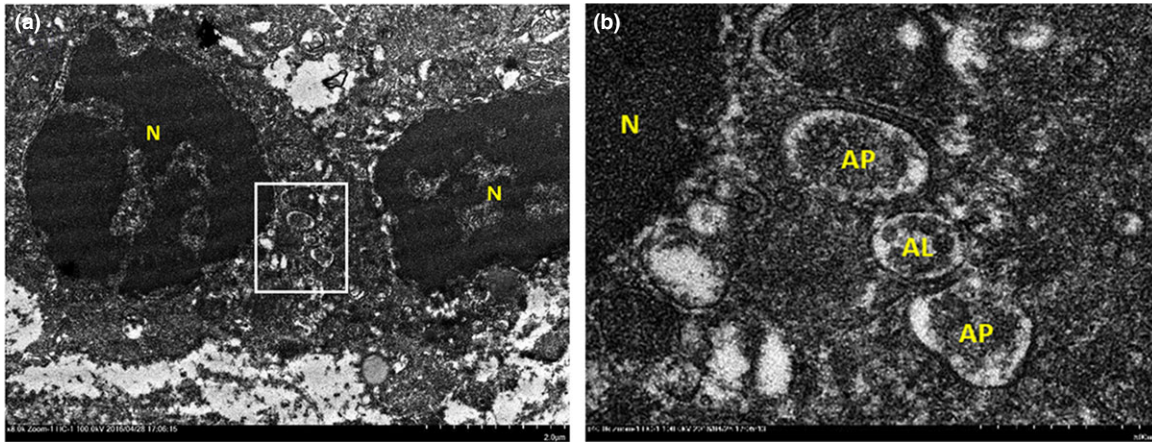


**Figure 10** (a) Representative ultrastructural morphology of autophagy in a radicular cyst by transmission electron microscopy (N: nucleus;  $\times 8000$ ); (b) double-membrane vacuoles were observed in the area denoted by a white square in (a) (AP: autophagosome; AL: autolysosome;  $\times 40,000$ ).

findings are compatible with a previous *in vitro* report stating that the cytoprotective role of autophagy that allows human dental pulp cells to resist hypoxia acts via the AMPK/mTOR pathway (Zhou *et al.* 2013).

In the present study, normal pulp tissue had low expressions of hypoxia-related proteins (pAMPK, HIF-1 $\alpha$  and BNIP3) according to both IHC and WB analyses. Although healthy teeth may not suffer severe hypoxic situations, it was speculated that mild hypoxia or nutrient depletion whilst using local anaesthesia could exist during tooth extraction. In the dental clinic, a local anaesthesia used in this study containing vasoconstrictors (2% xylocaine with 1 : 80,000 epinephrine) was used, and recent studies reported that there was potentially a short-term reduction in pulpal blood flow during anaesthesia (Odor *et al.* 1994, Gutmann 2010, Yoon *et al.* 2012). So, this might be one of the reasons for which a temporary hypoxic environment forms in extracted pulp tissue. Another reason may be related to the length of time from tooth extraction to storage of pulp tissue. As a matter of fact, the longer this time period, the more likely it is that hypoxia will form. As there were no inflammatory signs in any of the specimens of pulp tissue collected in the present study, healthy pulp tissues with some degree of hypoxia may be expected.

Whether autophagy exists in inflammatory periapical lesions and in normal pulp tissue was also investigated using immunostaining and immunoblotting. By immunostaining, positive staining for BECN1, LC3 and Atg5–12 proteins has been demonstrated in the epithelial lining of RCs, as well as in inflammatory

cells of cystic capsules and PGs, indicating that autophagy is potentially involved in the formation of inflamed periapical lesions. Significantly higher immunoscores for BECN1 and Atg5–12 in both RCs and PGs were noted ( $P < 0.05$ ) as compared to normal pulp tissue. In contrast to BECN1 and Atg5–12, a significantly lower immunoscore for LC3 was observed in RCs and PGs as compared to normal pulp tissue.

The aforementioned lower immunoscore for LC3 protein demonstrated by immunostaining in periapical lesions can be explained by the results of WB analysis. Indeed, LC3 protein consists of LC3I (16 kDa) and LC3II (14 kDa) subtypes with different molecular weights, LC3II having a relatively specific association with autophagosomes, indicating that it is an important marker of autophagic activity. Importantly, immunostaining cannot be used to differentiate the two different molecular weights of LC3I and LC3II due to limitations of the antibody used for immunostaining. So, the differential expressions of LC3I or LC3II could not be recognized in IHC staining. However, endogenous LC3 can be detected as two bands following SDS-PAGE and immunoblotting: one represents LC3I (16 kDa) the other LC3II (14 kDa) (Mizushima *et al.* 2007). In the immunoblotting experiments in the present study, a significantly lower expression of LC3I was observed in both periapical lesions as compared to normal pulp tissue, whilst a significantly higher expression of LC3II was noted in RCs and PGs than in normal pulp tissue. This could explain why the IHC expression of LC3 in normal pulp tissues was higher than that in the periapical

lesions, as demonstrated in the present study, because IHC staining detected the single form of LC3.

Recent studies confirmed that the amount of LC3II is closely correlated with the number of autophagosomes, serving as a good indicator of autophagosome formation, the amount of LC3II and the LC3II/LC3I ratio being able to be used to detect autophagy more appropriately (Mizushima & Yoshimori 2007). In the current study, not only was a significantly increased LC3II level in inflammatory periapical lesions observed, but also the ratio of LC3II/LC3I in both periapical lesions (LC3II/LC3I in PGs = 1.16; LC3II/LC3I in RCs = 1.24) was significantly higher than in normal pulp tissue (LC3II/LC3I = 0.06), implying that autophagy is potentially involved in the formation of inflammatory periapical lesions.

In the present study, the level of immunostaining of LC3 protein in normal pulp tissue was higher than that in inflamed periapical lesions, which was in contrast to the results of a previous study by Zhu *et al.* (2013), who reported stronger LC3 immunostaining in RCs and PGs as compared to normal pulp tissue. The aforementioned phenomenon demonstrated by Zhu *et al.* (2013) may be interpreted as evidence of the activation of autophagy; however, it may also be assumed that autophagy is suppressed, resulting in decreased autolysosome degradation of LC3 (Mizushima *et al.* 2010). Indeed, LC3 undergoes dynamic change during the autophagic process: during a short starvation period, the amount of LC3I decreases and that of LC3II increases; however, if cells are subjected to a longer period of starvation, both LC3I and LC3II disappear (Mizushima & Yoshimori 2007). This is because LC3II exists in the highest amounts when it is present both on inner and outer autophagosome membranes, and degradation of the inner membrane inside autolysosomes results in lower amounts of LC3II (forming a unique pattern called autophagic flux); meanwhile, LC3 on the outer membrane is deconjugated by Atg4 and returns to the cytosol (Tanida *et al.* 2005). As IHC analysis cannot distinguish the differential expressions of LC3I and LC3II, this method is unable to be used to explore the above-mentioned dynamic process between LC3I and LC3II upon autophagy identified in the study of Zhu *et al.* (2013).

The shortcoming of IHC in that it cannot discriminate the expressions of LC3I and LC3II could be addressed by the use of immunoblotting. The high expressions of Atg5-12, LC3II and BECN1 proteins, plus the higher ratio of LC3II/LC3I in periapical lesions (RCs and PGs) as compared to normal pulp

tissues, as determined in this study via WB analysis, could indicate elevated activity of autophagic processes under hypoxic and nutrient-depletion environments (Mizushima & Yoshimori 2007). Moreover, in normal pulp tissue, the present study was the first to demonstrate the high expression of LC3I and low expression of LC3II (and a low ratio of LC3II/LC3I), implying a low autophagic activity within normal pulp tissue that were not suffering hypoxia or nutrient depletion.

p62 is another good marker of the process of autophagic flux and can bind to LC3, serving as a selective substrate of autophagy (Bjørkøy *et al.* 2009, Barth *et al.* 2010). The level of p62 decreases during starvation in wild-type mouse embryonic fibroblasts (MEFs), but not in Atg5<sup>-/-</sup> MEFs (Kuma *et al.* 2004), suggesting that the reduction is mediated by autophagy. In addition, basal levels of p62 are upregulated in Atg5<sup>-/-</sup> MEFs, indicating that accumulation of p62 could be a good indicator of autophagy suppression (Wang *et al.* 2006, Nakai *et al.* 2007). So, in brief, the total cellular expression levels of p62 are inversely correlated with autophagic activity (Bjørkøy *et al.* 2005). Also, an elevated expression of LC3II and a high ratio of LC3II/LC3I, as well as a low p62 expression, suggests the induction of a functional autophagic process (Mizushima *et al.* 2010). In the current study, a decreased amount of p62 protein together with an elevated expression of LC3II and a high ratio of LC3II/LC3I in periapical lesions (RCs and PGs) was noted, which might imply that autophagic processes appeared to be functional in the periapical lesions.

The size of inflammatory periapical lesions of endodontic origin in terms of the mean diameter is usually found to be within 5–8 mm on periapical radiographic examination (Murphy *et al.* 1991, Sjögren *et al.* 1997). Traditionally, periapical lesions  $\leq 10$  mm were considered PGs, whilst lesions  $> 10$  mm were usually considered RCs (Lalonde 1970, Morse *et al.* 1973). In the present study, there were increased expressions of BECN1, LC3I, LC3II and p62 proteins in the group of periapical lesions  $> 10^2$  mm<sup>2</sup> as compared to the group of lesions  $\leq 10^2$  mm<sup>2</sup>, indicating that autophagy could potentially participate in the expansion of periapical lesions.

On the other hand, there were no significant differences (perhaps due to the small sample size) in the expressions of hypoxia- and autophagy-related proteins between the group of periapical lesions  $> 10^2$  mm<sup>2</sup> and the group of lesions  $\leq 10^2$  mm<sup>2</sup>. Interestingly, the expression trend in terms of lesions of

varying size was similar to the trend of protein expression in PGs and RCs. pAMPK was more highly expressed in the group of periapical lesions  $>10^2$  mm<sup>2</sup> and in the RC group. However, HIF-1 $\alpha$  was more highly expressed in the group of lesions  $\leq 10^2$  mm<sup>2</sup>, in addition to in the PG group. It might indicate that pAMPK could be predominantly involved in larger-sized periapical lesions (such as RCs), whilst HIF-1 $\alpha$  could be mainly involved in smaller-sized periapical lesions (such as PGs). This could also imply that there is a tendency of more active autophagy in large periapical lesions (such as RCs).

The exact mechanism of the formation of RCs is still not yet fully understood, although some authors have attempted to explain their pathogenesis (Gardner 1962, Shear 1963, Main 1970, Ten Cate 1972). The formation of RCs has been described as a process consisting of three phases (Shear & Speight 2007). During the first phase, the dormant epithelial cell-rests proliferate, probably due to the effects of inflammatory cytokines and growth factors (Lin *et al.* 2007) that are released by various cells residing in the apical lesion. During the second and third phases, an epithelium-lined cavity is formed and the cyst continues to grow. A major function of autophagy is to keep cells alive under stressful or hypoxic conditions, and hence, autophagy induction via hypoxia-related pathways is thought to participate in the development and maintenance of inflammatory periapical lesions. In the present study, autophagy and hypoxia were both proved to be present in inflammatory periapical lesions by immunoblotting, whereas autophagy was demonstrated in the epithelial cells of the cystic lining and the inflammatory cells of the capsule of RCs and PGs by immunostaining, which may imply autophagy potentially interacts with the immune and inflammatory responses, as well as protects the cystic epithelial lining and the epithelial rests of the capsule. Finally, the autophagic processes in inflamed periapical lesions in the present study were also verified by the findings of ultrastructures of autophagosomes and autophagic vacuoles in both RCs and PGs.

## Conclusion

The present study may be the first *in vivo* demonstration of both hypoxia and autophagy in inflamed periapical lesions of the jawbone. The results suggested that autophagy may play a potential causative role in the development and maintenance of periapical lesions which may be related to hypoxic or nutrient-

shortage environments. The presence of autophagy in the cystic epithelial lining may be associated with cystic development and expansion. These findings may present an additional concept of the pathogenesis of periapical lesions. Further studies (using cell cultures or animal models) to confirm the possible dual pathways (one via pAMPK/mTOR, another via HIF-1 $\alpha$ /BNIP3) of the induction of autophagy under hypoxia in the pathogenesis of inflamed periapical lesions are warranted.

## Acknowledgement

This work was funded by a grant (R103-16) from Ditmanson Medical Foundation Chia-Yi Christian Hospital. The authors gratefully acknowledge the director of Translational Medicine Research Center, Ying-Ray, Lee, and the Doctor, Chien-Chin, Chen of Pathological Department of Ditmanson Medical Foundation Chia-Yi Christian Hospital for excellent technical support.

## Conflict of interest

The authors have stated explicitly that there are no conflicts of interest in connection with this article.

## References

- Bando Y, Henderson B, Meghji S, Poole S, Harris M (1993) Immunocytochemical localization of inflammatory cytokines and vascular adhesion receptors in radicular cysts. *Journal of Oral Pathology & Medicine* **22**, 221–7.
- Barth S, Glick D, Macleod KF (2010) Autophagy: assays and artifacts. *Journal of Pathology* **221**, 117–24.
- Bernhardt WM, Wiesener MS, Weidemann A *et al.* (2007) Involvement of hypoxia-inducible transcription factors in polycystic kidney disease. *American Journal of Pathology* **170**, 830–42.
- Björkøy G, Lamark T, Brech A *et al.* (2005) p62/SQSTM1 forms protein aggregates degraded by autophagy and has a protective effect on huntingtin-induced cell death. *Journal of Cell Biology* **171**, 603–14.
- Björkøy G, Lamark T, Pankiv S, Øvervatn A, Brech A, Johansen T (2009) Monitoring autophagic degradation of p62/SQSTM1. *Methods in Enzymology* **452**, 181–97.
- Blouin CC, Page EL, Soucy GM *et al.* (2004) Hypoxic gene activation by lipopolysaccharide in macrophages: implication of hypoxia-inducible factor 1 $\alpha$ . *Blood* **103**, 1124–30.
- Dehne N, Brüne B (2009) HIF-1 in the inflammatory microenvironment. *Experimental Cell Research* **315**, 1791–7.
- Dery M, Michaud M, Richard D (2005) Hypoxia-inducible factor 1: regulation by hypoxic and non-hypoxic

- activators. *International Journal of Biochemistry and Cell Biology* **37**, 535–40.
- Dill A, Letra A, de Souza LC et al. (2015) Analysis of multiple cytokine polymorphisms in individuals with untreated deep carious lesions reveals IL1B (rs1143643) as a susceptibility factor for periapical lesion development. *Journal of Endodontics* **41**, 197–200.
- Eskelinen E-L (2005) Maturation of autophagic vacuoles in mammalian cells. *Autophagy* **1**, 1–10.
- Gardner A (1962) A survey of periapical pathology: part one. *Dental Digest* **68**, 162–7.
- Gutmann JL (2010) Local anesthetics, pulpal blood flow and C. Edmund Kells. *Journal of the History of Dentistry* **59**, 90–3.
- Hellwig-Burgel T, Rutkowski K, Metzen E et al. (1999) Interleukin-1beta and tumor necrosis factor-alpha stimulate DNA binding of hypoxia-inducible factor-1. *Blood* **94**, 1561–7.
- Kamada Y, Sekito T, Ohsumi Y (2004) Autophagy in yeast: ATOR-mediated response to nutrient starvation. In: Thomas G, Sabatini DM, Hall MN, eds. *TOR: target of Rapamycin*, 1st edn. Berlin, Heidelberg: Springer-Verlag, pp 73–84.
- Konisti S, Kiriakidis S, Paleolog EM (2012) Hypoxia—a key regulator of angiogenesis and inflammation in rheumatoid arthritis. *Nature Reviews Rheumatology* **8**, 153–62.
- Kuma A, Hatano M, Matsui M et al. (2004) The role of autophagy during the early neonatal starvation period. *Nature* **432**, 1032–6.
- Lalonde ER (1970) A new rationale for the management of periapical granulomas and cysts: an evaluation of histopathological and radiographic findings. *Journal of the American Dental Association* **80**, 1056–9.
- Lin LM, Huang GT-J, Rosenberg PA (2007) Proliferation of epithelial cell rests, formation of apical cysts, and regression of apical cysts after periapical wound healing. *Journal of Endodontics* **33**, 908–16.
- Lin LM, Ricucci D, Lin J, Rosenberg PA (2009) Nonsurgical root canal therapy of large cyst-like inflammatory periapical lesions and inflammatory apical cysts. *Journal of Endodontics* **35**, 607–15.
- Main D (1970) Epithelial jaw cysts: a clinicopathological reappraisal. *British Journal of Oral Surgery* **8**, 114–25.
- Mazure NM, Pouyssegur J (2010) Hypoxia-induced autophagy: cell death or cell survival? *Current Opinion in Cell Biology* **22**, 177–80.
- Meghji S, Qureshi W, Henderson B, Harris M (1996) The role of endotoxin and cytokines in the pathogenesis of odontogenic cysts. *Archives of Oral Biology* **41**, 523–31.
- Mizushima N, Yoshimori T (2007) How to interpret LC3 immunoblotting. *Autophagy* **3**, 542–5.
- Mizushima N, Yoshimori T, Levine B (2010) Methods in mammalian autophagy research. *Cell* **140**, 313–26.
- Moreau C, Devos D, Brunaud-Danel V et al. (2005) Elevated IL-6 and TNF- $\alpha$  levels in patients with ALS: inflammation or hypoxia? *Neurology* **65**, 1958–60.
- Morse DR, Patnik JW, Schacterle GR (1973) Electrophoretic differentiation of radicular cysts and granulomas. *Oral Surgery, Oral Medicine, Oral Pathology* **35**, 249–64.
- Murphy WK, Kaugars GE, Collett WK, Dodds RN (1991) Healing of periapical radiolucencies after nonsurgical endodontic therapy. *Oral Surgery, Oral Medicine, Oral Pathology* **71**, 620–4.
- Nair P, Sundqvist G, Sjögren U (2008) Experimental evidence supports the abscess theory of development of radicular cysts. *Oral Surgery, Oral Medicine, Oral Pathology, Oral Radiology, and Endodontology* **106**, 294–303.
- Nakai A, Yamaguchi O, Takeda T et al. (2007) The role of autophagy in cardiomyocytes in the basal state and in response to hemodynamic stress. *Nature Medicine* **13**, 619–24.
- Odor T, Pitt Ford T, McDonald F (1994) Adrenaline in local anaesthesia: the effect of concentration on dental pulpal circulation and anaesthesia. *Dental Traumatology* **10**, 167–73.
- Rabinowitz JD, White E (2010) Autophagy and metabolism. *Science* **330**, 1344–8.
- Ravikumar B, Futter M, Jahreis L et al. (2009) Mammalian macroautophagy at a glance. *Journal of Cell Science* **122**, 1707–11.
- Rubinsztein DC, Mariño G, Kroemer G (2011) Autophagy and aging. *Cell* **146**, 682–95.
- Sarbia M, Loberg C, Wolter M et al. (1999) Expression of Bcl-2 and amplification of c-myc are frequent in basaloid squamous cell carcinomas of the esophagus. *American Journal of Pathology* **155**, 1027–32.
- Shear M (1963) The histogenesis of the dental cyst. *Dental Practice* **13**, 238–43.
- Shear M, Speight P (2007) *Cyst of oral and maxillofacial regions*, 4th edn. Munksgaard: Blackwell.
- Sjögren U, Figdor D, Persson S, Sundqvist G (1997) Influence of infection at the time of root filling on the outcome of endodontic treatment of teeth with apical periodontitis. *International Endodontic Journal* **30**, 297–306.
- Tanida I, Minematsu-Ikeguchi N, Ueno T, Kominami E (2005) Lysosomal turnover, but not a cellular level, of endogenous LC3 is a marker for autophagy. *Autophagy* **1**, 84–91.
- Ten Cate A (1972) The epithelial cell rests of Malassez and the genesis of the dental cyst. *Oral Surgery, Oral Medicine, Oral Pathology* **34**, 956–64.
- Wang QJ, Ding Y, Kohtz S et al. (2006) Induction of autophagy in axonal dystrophy and degeneration. *Journal of Neuroscience* **26**, 8057–68.
- Westra J, Brouwer E, Bos R et al. (2007) Regulation of cytokine-Induced HIF-1 $\alpha$  expression in rheumatoid synovial fibroblasts. *Annals of the New York Academy of Sciences* **1108**, 340–8.
- Yoon M, Lee S, Kim E, Park S (2012) Doppler ultrasound to detect pulpal blood flow changes during local anaesthesia. *International Endodontic Journal* **45**, 83–7.

- Zhou S, Zhao L, Kuang M *et al.* (2012) Autophagy in tumorigenesis and cancer therapy: Dr. Jekyll or Mr. Hyde? *Cancer Letters* **323**, 115–27.
- Zhou Q, Liu H, Sun Q *et al.* (2013) Adenosine monophosphate-activated protein kinase/mammalian target of rapamycin-dependent autophagy protects human dental pulp cells against hypoxia. *Journal of Endodontics* **39**, 768–73.
- Zhu L, Yang J, Zhang J, Peng B (2013) The presence of autophagy in human periapical lesions. *Journal of Endodontics* **39**, 1379–84.

### Supporting Information

Additional Supporting Information may be found in the online version of this article:

**Figure S1.** Positive immunostaining of the positive control tissues (human breast carcinoma tissues) and negative staining of negative control tissues (human adipose tissues) for hypoxia-related proteins (HIF-1 $\alpha$ , pAMPK and BNIP3) (magnification:  $\times 200$ ). Scale bars = 100  $\mu$ m.

**Figure S2.** Positive immunostaining of the positive control tissues (human breast carcinoma tissues) and negative staining of negative control tissues (human adipose tissues) for autophagy-related proteins (BECN1, Atg5–12 and LC3) (magnification:  $\times 200$ ). Scale bars = 100  $\mu$ m.